

Rinderle, 1988). The F $_{\rm red}$ > peak is mainly associated with fluorescence emitted by PSII, while the F $_{\rm cfar-red}$ > peak consists of fluorescence emission from PSII and PSI. Therefore, the ratio (F_{ratio}) of red and far-red fluorescence might provide information about distinct environmental stress conditions. A meta-analysis by Ač et al. (2015) showed that water, temperature, and nitrogen stresses differ in their effect on F_{ratio}. A reduction of the leaf chlorophyll content, for example, results in an increase of the F_{ratio} on leaf and canopy level. F $_{\rm cfar-red}$ > generally increases with increasing chlorophyll concentration, while F $_{\rm red}$ > decreases due to re-absorption of the emitted F signal in this wavelength (Lichtenthaler et al., 1990; Rossini et al., 2015; Van Wittenberghe et al., 2013).

The most extensively used technique to measure fluorescence is the Pulse Amplitude Modulation (PAM), in this approach chlorophyll molecules are brought to excited states by absorption of active measurement light (Papageorgiou and Govindjee, 2004; Schreiber, 2004). Handheld Mini-PAM device allows for a quick assessment of leaf fluorescence whereas the stationary Monitoring-PAM is developed for continuous field measurements and can be clamped on leaf permanently as long as weather conditions or leaf growth allows. Upscaling this method to measure the canopy from above is limited by the close vicinity needed to apply a saturating light pulse. In recent years, the light-induced fluorescence transient method (LIFT, Kolber et al. (2005)) was developed. This method allows measurements of fluorescence parameters from a distance of several meters.

For large-scale studies, active methods will not be applicable and thus alternative methods to passively quantify the fluorescence emission have been developed. Such passive techniques retrieve chlorophyll fluorescence emission (termed sun-induced fluorescence, F) from the solar irradiance and the vegetation emitted radiance by using the absorption in the Earth's or solar atmosphere. In these absorption bands the incident irradiance is strongly reduced which allows the disentanglement of the relatively weak sun-induced fluorescence (less than 5% of APAR) and the reflected radiance. Due to their close spectral proximity to the peaks of the chlorophyll fluorescence emission spectrum, the two telluric O2 absorption bands - O2-B (687 nm) and O2-A (760.4 nm) - are used in this work to estimate F (Meroni et al., 2009). Analytical and technical developments nowadays allow fluorescence to be reliably measured using ground (Burkart et al., 2015; Cogliati et al., 2015; Guofang et al., 2018), airborne (Damm et al., 2014; Rascher et al., 2015; Wieneke et al., 2016; Zarco-Tejada et al., 2009), and satellite sensors (Frankenberg et al., 2014; Guanter et al., 2012; Joiner et al., 2011).

Several studies demonstrated that satellite-based F $_{<\,\mathrm{far}\text{-red}\,>}\,$ measurements can be linearly related with eddy covariance (EC) derived GPP (e.g. Frankenberg et al., 2011; Guanter et al., 2014; Sun et al., 2018). Satellite-derived F < far-red > has been retrieved from platforms/ instruments such as GOSAT (Greenhouse Gases Observing Satellite) (Frankenberg et al., 2011; Guanter et al., 2012; Joiner et al., 2012, 2011), GOME-2 (Global Ozone Monitoring Instrument 2) (Joiner et al., 2013; Köhler et al., 2015), SCIAMACHY (SCanning Imaging Absorption SpectroMeter for Atmospheric CHartographY) (Köhler et al., 2015), and OCO-2 (Sun et al., 2018). Since the primary objective of these missions is to track atmospheric trace gases, data have to be spatially and temporarily aggregated, which results in F $_{<\,{\rm far\text{-}red}\,>}\,$ images with coarse spatial (0.5° for GOSAT and GOME-2, 2.25 \times 1.29 km for OCO-2) and biweekly to annual temporal resolution. Recently it has been questioned if the relationship between GPP and satellite retrieved F < farred > is solely driven by their common dependence on the photosynthetic active radiation (PAR) and the fraction of absorbed PAR (fAPAR), or if F can be also related to the photosynthetic light- and dark reactions (light use efficiency; LUE) (Du et al., 2017; Guofang et al., 2018; Li et al., 2018; Zhang et al., 2018). Due to the technical constrains of space- and air-borne sensors, long-term in-situ measurements are needed to fully understand the diurnal adaptive and competitive

energy (Maxwer to properly estimate GPP (r the xanthophyll cycle and the associated retion by NPQ generates an optical signal, which can be dereflectance around 531 nm. The photochemical reflectance index (PRI) exploits the changes in reflectance at 531 nm and a reference wavelength at 570 nm to assess light use efficiency (LUE; defined as the amount of assimilated CO2 molecules per absorbed photon) based on its relationship with NPQ (Gamon et al., 1992). Even though several studies demonstrated the potential of PRI as a remote sensing proxy for LUE (Drolet et al., 2008, 2005; Peñuelas et al., 2011; Rossini et al., 2010), the use of PRI to detect NPQ is complicated by several factors. It is shown that the PRI is affected by canopy structure (Barton and North, 2001; Drolet et al., 2005; Gamon, 2015; Wu et al., 2010) and temporal changes in leaf pigments (Gamon et al., 2001; Sims and Gamon, 2002). These effects influence the stand photosynthetic rate, which can produce changes in the PRI-photosynthesis relationship that are independent of the xanthophyll cycle and consequently result in a misinterpretation of the PRI-NPQ relationship (Alonso et al., 2017; Gitelson et al., 2017).

In this study, one of the first high-resolution time-series of red (retrieved at 687 nm; F_{687}) and far-red (retrieved at 760 nm; F_{760}) fluorescence, measured every 6 s over a period of two months during the heatwave in summer 2015 is presented. A micrometeorological station, designed for EC measurements, was located within the study field to track CO_2 and water fluxes. The availability of simultaneous spectral and EC measurements allowed analyzing if F can be related to the photosynthetic light- and dark reactions or if it merely relates to GPP due to their common dependence on APAR. Furthermore, the far-red fluorescence yield and the photochemical reflectance index are corrected for seasonal changes in the canopy structure to analyze the diurnal and seasonal relationships between LUE, FY and PRI (as an indicator for NPQ).

2. Materials and methods

2.1. Study area

The measurement campaign was conducted close to the village of Merzenhausen (50°55′ N, 6°17′ E, 92 m a.s.l.), which is located in the Rur catchment in the central western part of North Rhine-Westphalia, Germany. The study site belongs to the TERENO network (Zacharias et al., 2011). It covers a 6.9 ha (approx. $200 \,\mathrm{m} \times 300 \,\mathrm{m}$) conventionally managed agricultural field with the typical crop rotation of the region, including two seasons of winter wheat and one season of sugar beet. During the measurement campaign the field was planted with sugar beets (Beta vulgaris subsp. vulgaris). The field soil texture is classified as silt loam (Graf et al., 2013). Sowing happened in mid of April (day of year (DOY): 103), and harvest in end of October (DOY: 302). Ground measurements started 28 of June (DOY: 179), when the rosette growth was already completed and the leaves covered at least 90% of the ground (BBCH-Code: 39 - the Biologische Bundesanstalt, Bundessortenamt und CHemische Industrie), and ended 31 of August (DOY: 243) shortly before harvest. The regional temperature in July and August amounts on average for 18 °C, while the averaged maximum temperature is 23 °C. The average precipitation for July and August is 79 and 76 mm respectively. The first month of the campaign (July), the region was strongly affected by the 2015 summer heatwave (Orth et al., 2016), resulting in an average temperature of 22 °C and an averaged maximum temperature of 24 °C. The precipitation differed strongly between July (39 mm, 50% of the climatological average) and August (76 mm).

2.2.1. Measurements of CO2 fluxes and meteorological data

Meteorological and flux measurements were recorded at a micrometeorological tower located in the center of the study site, close to the field spectrometer setup. The tower was equipped with turbulence sensors for measuring the net ecosystem exchange of CO2 (NEE) (Baldocchi, 2003). Wind components were obtained with a sonic anemometer at 2 m above surface (CSAT3, Campbell Scientific, Inc., Logan, USA). At the same height CO2 concentrations were measured using an open-path infrared gas analyzer (LI7500, LI-COR Inc., Lincoln, NE, USA). Data of both instruments were recorded with a logger (CR3000, Campbell Scientific, Logan, UT, USA) at 20 s⁻¹. The post field processing of fluxes was performed with the TK3.1 software (Mauder & Foken, 2015), using the standardized TERENO strategy for EC data calculation and quality assurance presented in detail by Mauder et al. (2013). It includes well-established conversions, corrections, and plausibility tests that lead into 30-minute flux estimates of NEE labeled as high, moderate, and low-quality data. For this study, only high quality data was used, low and moderate data were treated as missing values. Based on the wind direction the cumulative source contribution of the target field was calculated. For selected clear sky days (c.f. Section 3.1) 83-96% of the measured fluxes laid within the study field. Finally, a combined gap filling and flux partitioning algorithm according to Reichstein et al. (2005), was applied to all remaining NEE data to receive a continuous time series of gross primary production

The LUE describes how much carbon is assimilated by incoming photon (μ mol CO_2/μ mol photon) and was calculated as:

$$LUE = \frac{GPP}{APAR} \tag{1}$$

GPP was derived from flux measurements of the EC tower and APAR from the spectrometer system (*SIF-Sys*; cf. Section 2.2.2). Since no transmitted PAR measurements were available, APAR was calculated from the difference between incident and reflected radiance, integrated over the spectral region from 400 nm to 700 nm (Li and Moreau, 1996).

The evapotranspiration (ET, in mm/30 min) was calculated as:

$$ET = \frac{LE \cdot 1800}{(\Delta Q_{\nu} - 0.00242 \cdot T) \cdot 10^{6}}$$
 (2)

where LE is the latent heat flux derived from the EC tower, T the air temperature (in Celsius) at 2 m above ground and ΔQ_v the specific heat evaporation (2.498 MJ) at 0 °C. Along with EC fluxes, the main meteorological variables were constantly measured and integrated over 30 min. The temperature (T) and the absolute humidity were measured with a shielded probe (HMP45C, Vaisala Inc., Helsinki, Finland) at 2 m above ground level. The precipitation was measured by a tipping bucket rain gauge (RM Young 52203, R.M. Young Company, Traverse City, USA) and the volumetric water content (VWC) with two water content reflectometers (CS616, Campbell Scientific, Inc., Logan, USA) at a depth of 2.5 cm.

2.2.2. High-resolution spectroscopy to measure top-of-canopy fluorescence

The automated field spectrometer system (*SIF-Sys*) is a successor of earlier developments of the Forschungszentrum Jülich and the University of Milano Bicocca (Cogliati et al., 2015; Julitta et al., 2016; Rossini et al., 2010). *SIF-Sys* consists of one QEPro (Ocean Optics, Dunedin, FL, USA) spectrometer with a spectral resolution of 1 nm FWHM (full width at half maximum), a spectral sampling interval (SI) of 0.3 nm and a signal to noise ratio (SNR) of 1000:1 in a spectral range from 300 to 1000 nm. The QEPro is connected to an optical multiplexer (MPM-2000, Ocean Optics, Dunedin, FL, USA) which allows switching between a channel measuring the incident irradiance (up-looking cosine response optic), the upwelling radiance (down-looking bare optic; 25° field of view) and a blind channel for the spectral dark current

ware

spectral data on a...

three temperature sensors, one out in parallel. To ensure stable measure

meter is housed in a separated and actively cooled insurated

The instrument was mounted on a 2 m high tower resulting in a footprint of around 50 cm. The technical description and evaluation can be found in Burkart et al. (2015).

Measurements started every day at 6 a.m. and lasted until 4 p.m. UTC. The optical path of the system is optimized for high light-throughput aiming to decrease the integration time and thus increase the signal-to-noise level. With this fast acquisition time (ca. 6 s.), around 5000 measurements per day are possible. The retrieval of F was conducted in the $\rm O_2A$ and $\rm O_2B$ oxygen absorption bands, by using the improved Fraunhofer line depth (iFLD) retrieval method. The iFLD method is based on the FLD method (Plascyk and Gabriel, 1975) and estimates F by incorporating correction coefficients to improve the description of reflectance and fluorescence spectral characteristics (Alonso et al., 2008). Since diffuse light conditions strongly affect the fluorescence retrieval (Damm et al., 2015), only measurements under clear sky conditions were selected (22 days) (Sub. Fig. 1). The average and standard error of the fluorescence and reflectance measurements were then computed for each minute.

Analog to the LUE, the emission efficiency of fluorescence is referenced as FY. FY indicates the fraction (% nm $^{-1}$) of photons that are reemitted in relationship to the absorbed photons. Since F_{687} was strongly affected by reduced reabsorption effects only FY at 760 nm (FY₇₆₀) was calculated as:

$$FY_{760} = \frac{F_{760}}{APAR} \cdot 100 \tag{3}$$

Assuming a Lambertian behavior of the fluorescence emission, F_{760} radiance was converted to irradiances multiplying by π and then to μ mol m⁻²s⁻¹nm⁻¹, calculating the number of photons at the specific wavelength.

The fluorescence ratio was calculated by dividing red fluorescence by far-red fluorescence:

$$F_{ratio} = \frac{F_{687}}{F_{760}} \tag{4}$$

2.2.3. Remotely sensed vegetation indices

To analyze the effect of seasonal changes in canopy structure and chlorophyll content, additional vegetation indices (VIs) were calculated. The modified triangular vegetation index (MTVI2) was used to track changes in green LAI minimizing the effect of variations in leaf chlorophyll content (Haboudane et al., 2004). The MTVI2 was calculated as:

$$MTVI2 = \frac{1.5[1.2(R_{800} - R_{550}) - 2.5(R_{670} - R_{550})]}{\sqrt{(2R_{800} + 1)^2 - (6R_{800} - 5\sqrt{R_{670}}) - 0.5}}$$
(5)

where R_{λ} is the reflectance at the given wavelength λ .

The chlorophyll vegetation index (CVI) was developed by Vincini et al. (2008) for estimating leaf level chlorophyll content in planophile plants with a reduced sensitivity towards structural effects. The CVI was calculated as:

$$CVI = \frac{NIR}{Green} \cdot \frac{Red}{Green}$$
 (6)

The CVI uses the average reflection in the spectral range of 520–600 nm (green), 630–690 nm (red) and 760–900 nm (NIR).

The photochemical reflectance index (PRI) was used to obtain information about the xanthophyll cycle activity, which is linked to the release of energy as heat (NPQ) (Gamon et al., 1992). The PRI was calculated as:

$$RM = \frac{R_{570} - R_{531}}{R_{570} + R_{531}} \tag{7}$$

where R_{531} is the xanthophyll sensitive reflectance at 531 nm and R_{570} the reference reflectance at 570 nm. An increased PRI indicates therefore an increased activity of the xanthophyll cycle.

2.2.4. Data post processing and F uncertainty

Outliers (values above/below \pm 3 σ) were removed and all parameters derived from the spectrometer were aggregated from 1 min to 30 min to match the EC measurements. Measurements with a solar zenith angle (SZA) over 60° were excluded for the full dataset, while measurements under diffuse light conditions were only excluded for the APAR relative yield analysis. The fluorescence measurement uncertainty was defined as the standard deviation over 1 min windows. The averaged, minimum and maximum relative uncertainty of F_{760} was found to be 6.6, 5.8 and 7.6% respectively. The averaged, minimum and maximum relative uncertainty of F_{687} was with 21%, 17% and 28% respectively. With decreasing SZA and increasing APAR, the uncertainty slightly increased (Sub. Fig. 2).

2.2.5. Correction of seasonal effects on PRI and FY₇₆₀

PRI and FY were corrected for stress and phenological related seasonal changes of the canopy structure by using an adapted version of a de-trending method developed by Wu et al. (2015) on PRI measurements. They calculated a structural-related PRI (sPRI) as a function of the leaf area index (LAI), with the assumption that the residual PRI (rPRI = PRI – sPRI) would be independent from structural effects.

As there was no access to LAI measurements the rPRI and residual FY_{760} (rFY₇₆₀ = FY_{760} – sFY_{760}) were calculated by using the daily mean MTVI2 as a proxy for LAI, where the model describing best the relationship between MTVI2 to PRI ($R^2 = 0.94$) and MTVI2 to FY_{760} ($R^2 = 0.88$) are:

$$sPRI = 0.31 - 0.18 \cdot (1 + MTVI2)$$
 (8)

$$sFY_{760} = 0.06 \cdot MTVI2$$
 (9)

3. Results

3.1. Stress day selection

The detection of days with environmental stress conditions, was based on the light response curve of GPP, the diurnal mean VWC of the upper soil layer and the diurnal mean ET rate. As shown in Fig. 1 GPP increased linearly with increasing APAR if the high ET rates can be compensated by available soil water. These days were associated to non-stress conditions (NSC). If the water loss due to increased ET rates cannot be compensated by available soil water, the $\rm CO_2$ assimilation saturates even though APAR increases. These days were defined as days under stress conditions (SC).

3.2. Seasonal cycle

The seasonal evolution of measured variables was strongly affected by a heatwave that struck central Europe in summer 2015 (Orth et al., 2016). As described in Section 3.1 the measurement season was classified into days under SC (Fig. 2, red areas) and NSC (Fig. 2, blue areas). The SC days were characterized by high temperatures (Fig. 2A dots), high ET rates, low LUE, and low VWC. Fluctuations in GPP, F_{760} , and F_{687} were mainly driven by changes in APAR (Fig. 2B), while LUE, F_{760} , and F_{687} showed a stronger response to drought stress. For days under clear sky conditions the LUE showed only a small increase until DOY 219. Only after the strong rain event around DOY 227 the water availability increased enough to allow a significant gain in LUE. In contrast to F_{760} , the F_{760} (Fig. 2C) increased over the measurement period and showed a behavior similar to MTVI2. The CVI, as an

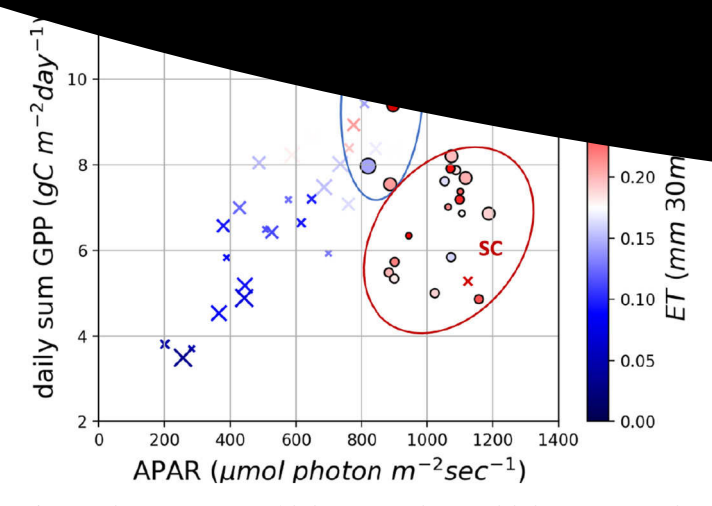


Fig. 1. Light response curve of daily aggregated GPP and daily mean APAR. The x's mark measurements under diffuse light conditions, circles mark measurements under relatively clear sky conditions. The size of the symbols indicates the soil water content (SWC, smallest 10 vol%, biggest 26 vol%). Points within the blue circle symbolize measurements under non-stress conditions (NSC). Points within the red circle symbolize measurements affected by stress conditions (SC). The color gradient indicates the evapotranspiration rate from 0 to 0.35 mm 30 min ⁻¹. (For interpretation of the references to color in this figure legend, the reader is referred to the web version of this article.)

indicator for leaf chlorophyll content, increased over time with highest values at the end of the measurement period. The seasonal changes in the canopy structure (indicated by MTVI2) and chlorophyll content affected the uncorrected PRI, which showed a constant decrease over the measurement season (Fig. 2D).

3.3. Relationship of F_{760} and F_{687} to GPP and APAR

In the following sections the 30 min dataset is referred to as intradaily data and the daily averaged dataset as seasonal data. Results showed under NSC a moderate linear relationship between intra-daily and seasonal GPP to $F_{760}\ (R^2=0.57$ and 0.72) as well as to $F_{687}\ (R^2=0.45$ and 0.48). When affected by SC these relationships significantly decrease for $F_{760}\ (R^2=0.07$ and non-significant) and $F_{687}\ (R^2=0.04$ and non-significant) (Fig. 3A/B & E/F).

Furthermore Fig. 3 showed that intra-daily and seasonal F_{760} ($R^2=0.96$ and 0.97) and F_{687} ($R^2=0.84$ and 0.76) related under NSC more strongly to APAR than to GPP. Under SC the intra-daily and seasonal relationship between F_{760} to APAR decrease strongly ($R^2=0.42$ and non-significant). While the intra-daily relationship between F_{687} and APAR showed no significance under SC, the seasonal relationship inverted to a negative one ($R^2=0.60$).

3.4. Relationship of FY_{760} and F_{ratio} to LUE

In order to analyze the contribution of regulatory processes in photosynthesis that are independent of APAR, the relationships between light use efficiency (LUE) derived from EC towers, FY $_{760}$ and the F $_{\rm ratio}$ were analyzed. Due to the strong reabsorption effects of red fluorescence, and since no correction method was available, FY $_{687}$ was not analyzed in this work. The intra-daily and seasonal relationship between FY $_{760}$ and LUE showed a logarithmic increase over the full measurement period (R 2 = 0.64 and 0.79 respectively) (black line, Fig. 4A & C), while intra-daily and seasonal F $_{\rm ratio}$ decreased exponentially with increasing LUE (R 2 = 0.45 and 0.52 respectively) (black line, Fig. 4B & D). These relatively strong relationships are defined by the two distinctive responses of sugar beet under NSC and SC. Under SC a fast linear increase of FY with increasing LUE is generally

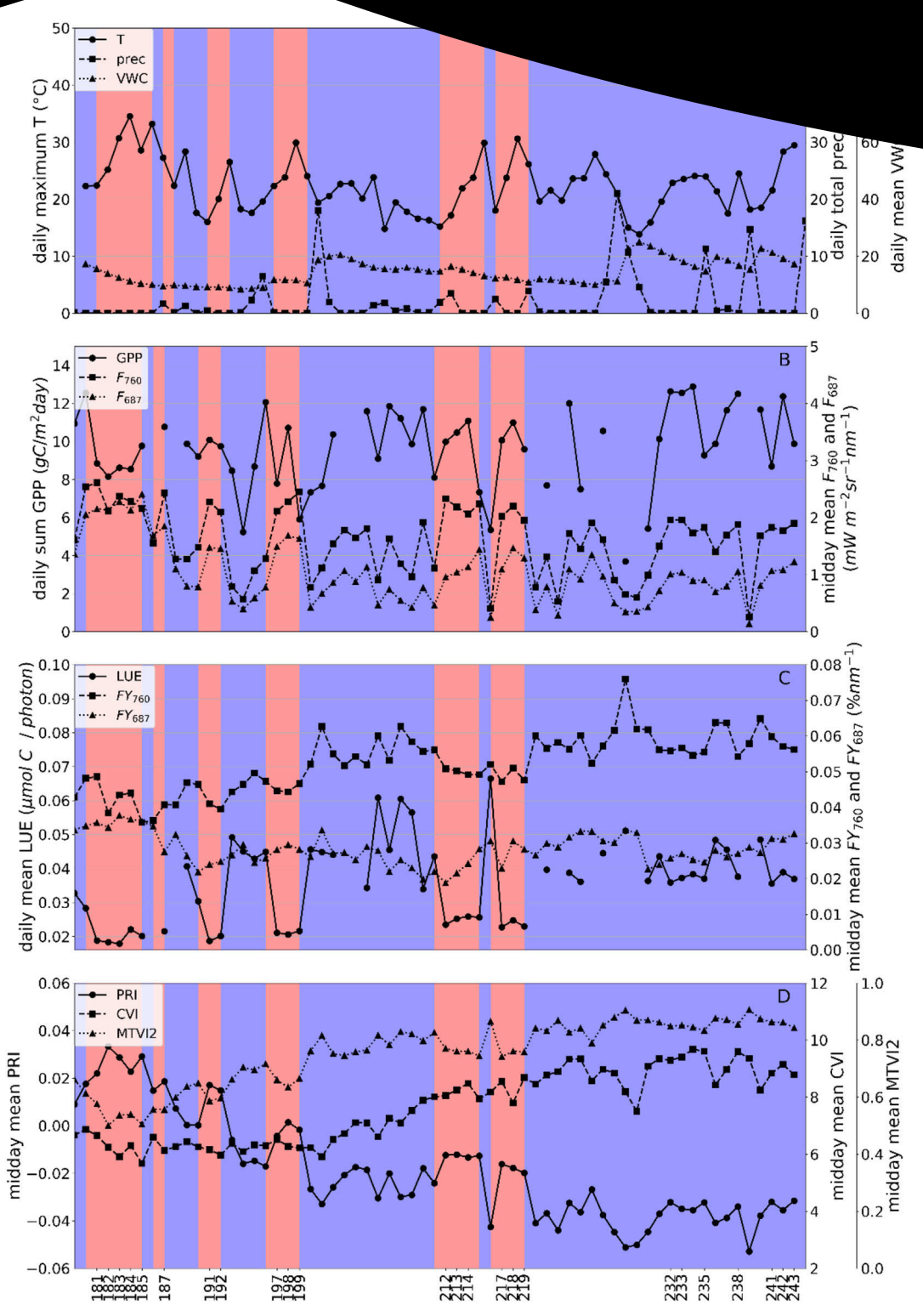


Fig. 2. Seasonal course of daily maximum temperature (T; dots in panel A), daily sum precipitation (prec; squares in panel A), daily mean volumetric water content (VWC; triangles in panel A) daily sum gross primary production (GPP; dots in panel B), midday mean fluorescence at 760 nm (F_{760} ; squares in panel B), midday mean fluorescence at 687 nm (F_{687} ; triangles in panel B), daily mean light use efficiency (LUE; dots in panel C), midday mean F yield (FY₇₆₀ and FY₆₈₇; squares and triangle in panel C), midday mean photochemical reflectance index (PRI; dots in panel D), midday mean chlorophyll vegetation index (CVI; squares in panel D), midday mean modified triangular vegetation index (MTVI2; triangle in panel D). The red plot background color symbolize days affected by stress conditions (SC) and the blue plot background color symbolize non-stress conditions (NSC). (For interpretation of the references to color in this figure legend, the reader is referred to the web version of this article.)

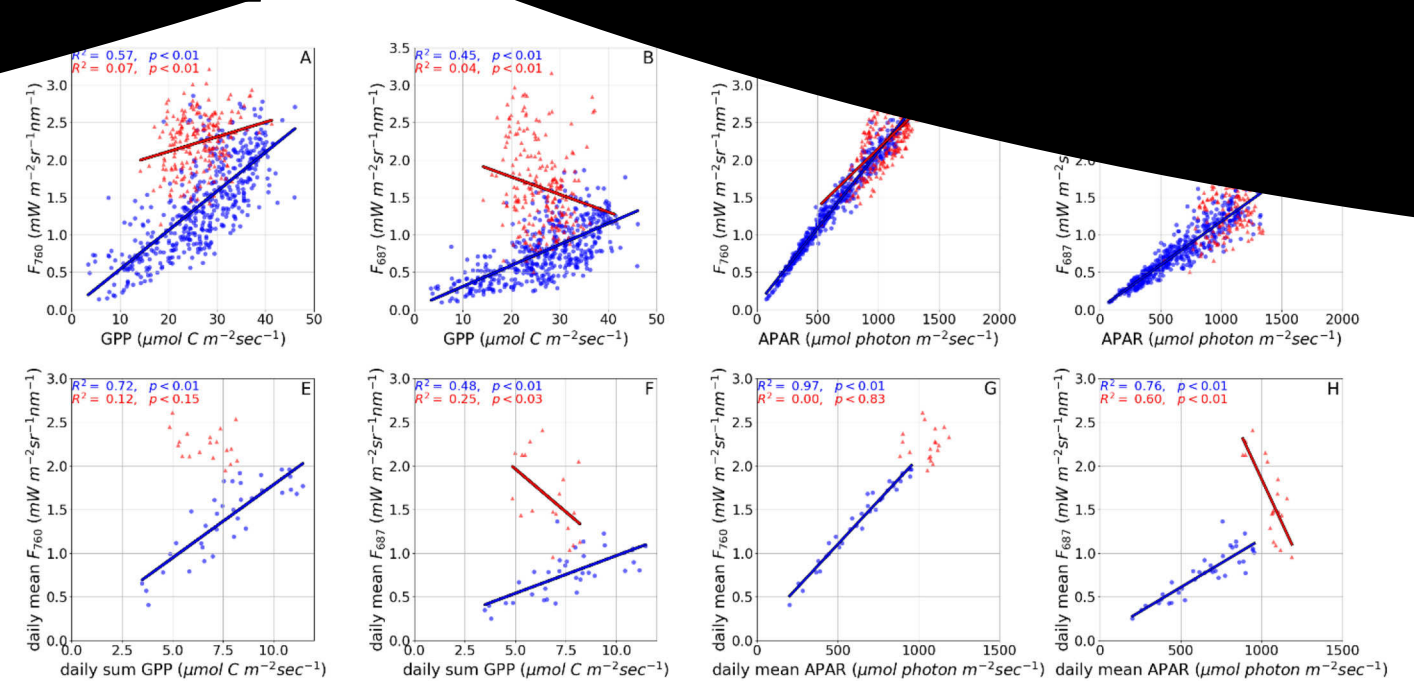


Fig. 3. Intra-daily (A–D) and seasonal (E–H) relationship of F_{760} and F_{687} , to GPP and APAR within a sugar beet field, in 2015 Merzenhausen, Germany. Red dots represent measurements affected by stressed conditions (SC). Blue dots represent measurements under non-stressed conditions (NSC). The red lines represent the best model fit for measurements affected by SC and the blue lines the best model fit for measurements under NSC. (For interpretation of the references to color in this figure legend, the reader is referred to the web version of this article.)

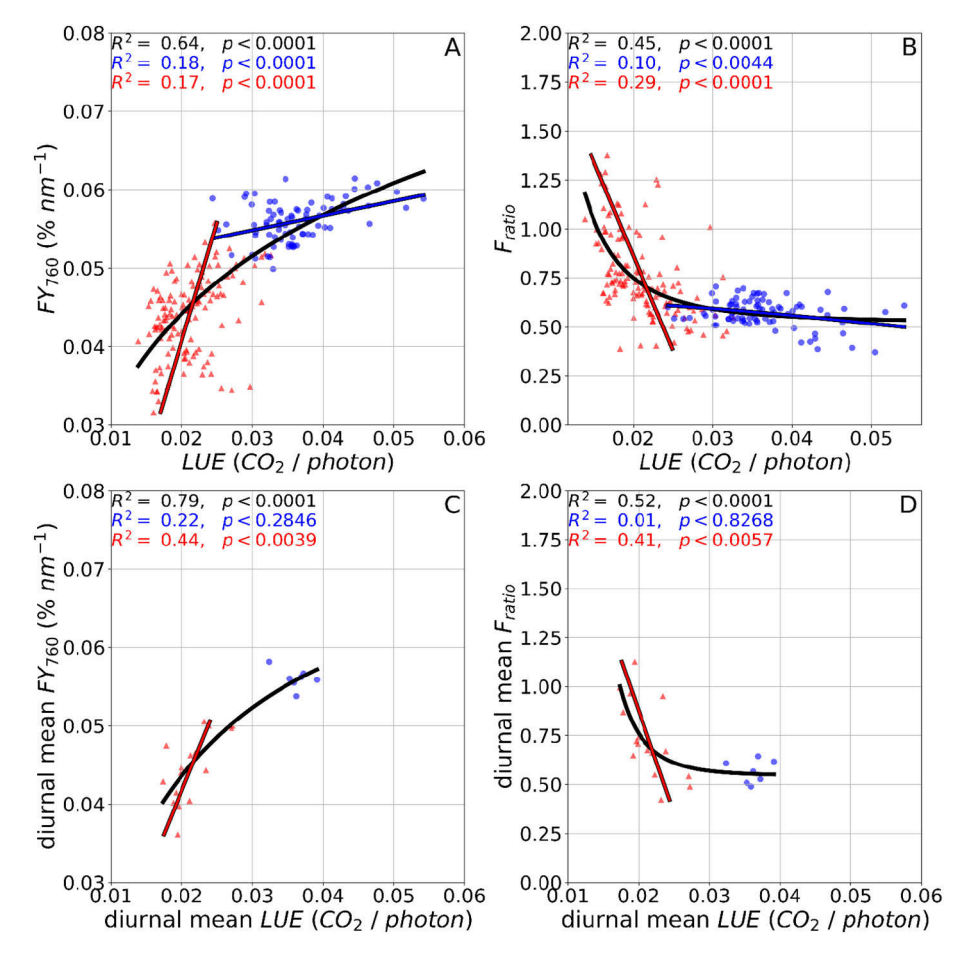
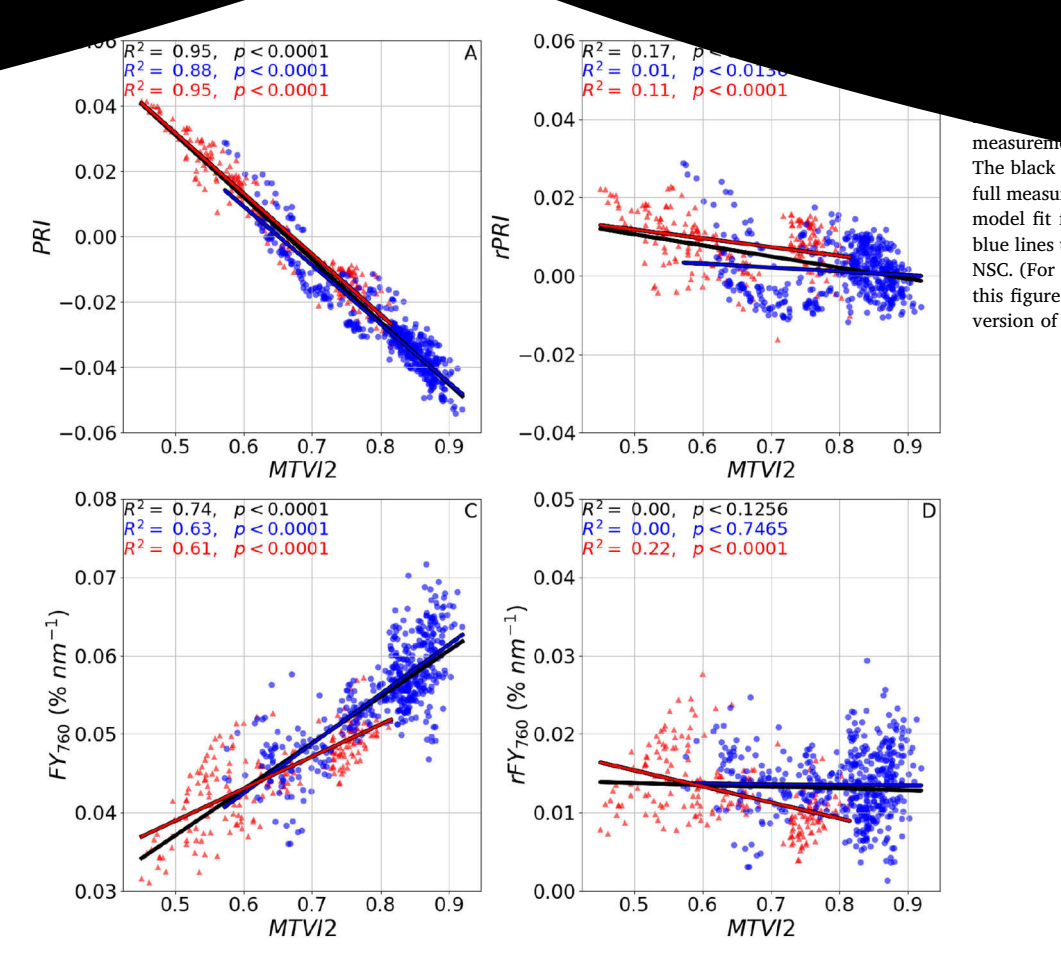


Fig. 4. Intra-daily and seasonal relationship of FY₇₆₀ and F_{ratio} with LUE within a sugar beet field, in 2015 Merzenhausen, Germany. Red dots represent measurements affected by stressed conditions (SC). Blue dots represent measurements under non-stressed conditions (NSC). The black lines represent the best model fit over the full measurement season, red lines represent the best model fit for measurements affected by SC and the blue lines the best model fit for measurements under NSC. (For interpretation of the references to color in this figure legend, the reader is referred to the web version of this article.)



The black lines represent the full measurement season, red lines represent the model fit for measurements affected by SC and the blue lines the best model fit for measurements under NSC. (For interpretation of the references to color in this figure legend, the reader is referred to the web version of this article.)

observed, while under NSC this increase slowed down (red and blue line, Fig. 4A & C). Under NSC, $F_{\rm ratio}$ increased slowly with decreasing LUE, while under SC $F_{\rm ratio}$ increased strongly with decreasing LUE (red and blue line, Fig. 4B & D). It was found that MTVI2 (CVI) explained 59% (50%) of the variance in $F_{\rm ratio}$ (Sub. Fig. 3).

3.5. Influence of seasonal changes in canopy structure on PRI and FY₇₆₀

Results showed that both PRI and FY_{760} are strongly related to the MTVI2 (LAI proxy, Fig. 5A & C; $R^2=0.95$ and 0.74 respectively). By calculating the residual PRI (rPRI) and residual FY_{760} (rFY₇₆₀) (c.f. Section 2.2.5) the stress and phenology-related influence of the changing canopy structure was removed. The relationship between rPRI and MTVI is thereby reduced ($R^2=0.14$) and the one between rFY₇₆₀ and MTVI2 becomes non-significant. It is important to note that the detrending method does not correct for diurnal changes in the canopy structure, which caused the strong variance shown in Fig. 5B & D. As stated in Section 1 the PRI is not only affected by structural effects but also by changes in leaf pigments. Supplementary Fig. 4 shows that the correction method based on MTVI2 also reduced the relationship with the chlorophyll sensitive CVI.

3.6. APAR and seasonally de-trended relationship of rFY $_{760}$, rPRI, and LUE

Fig. 6A showed a distinct relationship of rFY_{760} to LUE for the intradaily NSC and SC. Under SC, when LUE is lowest, rFY_{760} showed large dispersion, while under NSC rFY_{760} increased linearly with increasing LUE but with high variability. Intra-daily rPRI increased under NSC and SC linearly with decreasing LUE (R^2 : 0.58 and 0.46). Under NSC, rFY_{760} decreased with increasing rPRI (R^2 : 0.22), while under SC rFY_{760} showed no relationship with rPRI.

Under NSC and SC seasonal rFY_{760} decreased linearly with increasing LUE (R²: 0.65 and 0.34) (Fig. 6D). No significance was found between seasonal rPRI and LUE (Fig. 6E) as well as between rFY_{760} and rPRI (Fig. 6F). Furthermore, it is observed that under SC rFY_{760} values are generally higher than under NSC. This behavior is opposite to the one found for uncorrected FY_{760} (Fig. 4).

3.7. Diurnal relationship of rFY₇₆₀, rPRI and LUE

For a better understanding of the diurnal interactions between rFY760, rPRI and LUE, the mean diurnal cycle and their relationships during NSC (Fig. 7; blue lines) and SC (Fig. 7; red lines) are compared. By calculating the average of 7 days under NSC and 17 days under SC we reduce for diurnal structural effects of the canopy. Under NSC, LUE decreases from morning until 1 h after solar noon with a subsequent fast increase. Analog to the LUE, rFY760 decreases strongly from morning until solar noon. Right after solar noon rFY760 strongly increases with increasing LUE. The rPRI reaches its highest values around 1.5 h before solar noon and stays relatively stable until 1.5 h after solar noon, when it starts decreasing. Similar to the NSC the LUE reaches under SC its lowest values 1 h after solar noon. The subsequent increase however, happens at a much slower rate than under NSC. The rFY₇₆₀ decreases until 1.5 h before solar noon and stays then relatively stable until 2.5 h after solar noon. The rPRI on the contrary increases until 1 h before solar noon, stays stable until 2h after solar noon and subsequently decreases rapidly (Fig. 7A-C).

The trajectories of the mean diurnal relationships (Fig. 7D–F) show that under SC rFY_{760} and rPRI are linearly related to the LUE and to each other. Under NSC however, these relationships are not that strongly pronounced. Around solar noon a clustering of rFY_{760} , LUE, and rPRI under SC and NSC is observed. Interestingly, the positive

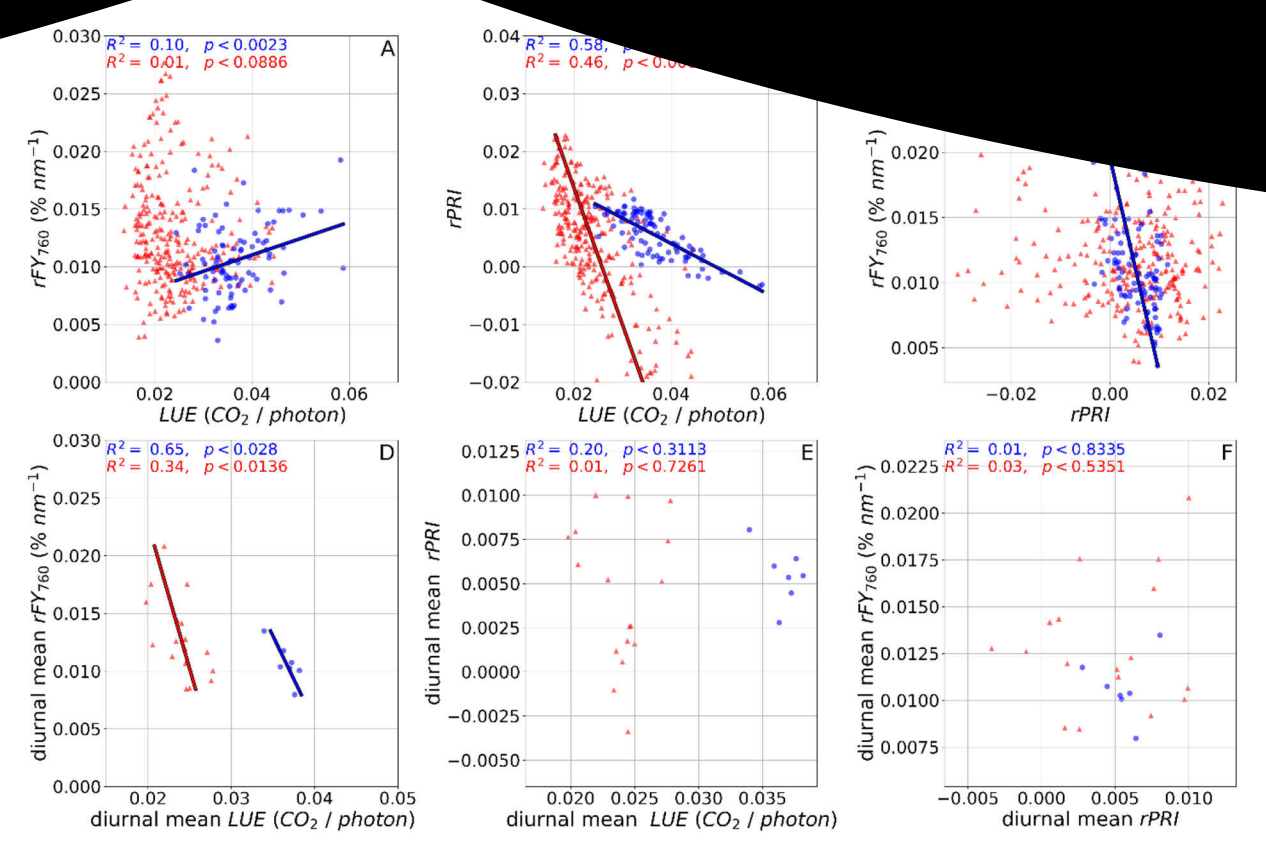


Fig. 6. Intra-daily and seasonal relationship between rFY_{760} , rPRI and LUE within a sugar beet field, in 2015 Merzenhausen, Germany. Red dots represent measurements affected by stressed conditions (SC). Blue dots represent measurements under non-stressed conditions (NSC). Red lines represent the best model fit for measurements affected by SC and the blue lines the best model fit for measurements under NSC. (For interpretation of the references to color in this figure legend, the reader is referred to the web version of this article.)

relationship between rFY $_{760}$ and LUE (Fig. 7D) contradicts the negative relationship between seasonal rFY $_{760}$ and LUE (Fig. 6D) described in Section 3.6.

4. Discussion

4.1. The influence of APAR on the relationship between GPP and F

The results are in agreement with several studies that showed that under NSC F₇₆₀ linearly increases with GPP (Cheng et al., 2013; Frankenberg et al., 2011; Goulas et al., 2017; Guanter et al., 2012, 2014; Zhang et al., 2016). However, when the sugar beet was affected by environmental stress conditions the relationship between F₇₆₀ and F₆₈₇ to GPP reduced significantly (Fig. 3A & B). It is assumed that the lower relationship between F and GPP is related to structural changes of the canopy but also a dominant release of energy as heat (NPQ) (Fig. 7) (Porcar-Castell et al., 2014). The strong increase in F₆₈₇ during the stress phase can be related to reduced reabsorption effects of red fluorescence due to chronic stress responses like reduced chlorophyll content, leaf rolling and leaf wilting (Fournier et al., 2012; Rossini et al., 2015; Van Wittenberghe et al., 2015). It is furthermore shown that F760 and F687 are more strongly related to APAR than to GPP (Fig. 3). This finding supports the assumption that the relationship between F and GPP is primarily driven by APAR (Du et al., 2017; Goulas et al., 2017; Li et al., 2018; Zhang et al., 2016).

As described in the introduction, several studies showed a linear relationship between satellite-based F $_{<\,\mathrm{far-red}\,>}$ and eddy covariance (EC) derived GPP. Our results partly contradict such linear relationship and corroborate the hypothesis that the relationship between fluorescence and GPP is not as simple. We demonstrate that under non-stress conditions, fluorescence at 760 nm has indeed a linear relationship with

GPP (Fig. 3). However, under stress conditions no linear relationship between GPP and fluorescence at 687 or 760 nm was found (Fig. 3).

4.2. Intra-daily and seasonal relationship of FY_{760} and F_{ratio} with LUE

It was found that intra-daily and seasonal FY_{760} share a relatively strong logarithmic relationship with LUE. This relationship however is defined by the two distinctive linear relationships between FY_{760} to LUE under NSC and SC (Fig. 4). Furthermore, it is shown that FY_{760} shares an even stronger relationship with MTVI2, which implies that the relationship between FY_{760} and LUE is mainly driven by stress and phenological induced changes of the canopy structure (Fig. 5). It has to be noted that the calculation of APAR is based on the reflected radiance measured by the spectrometer. Therefore, APAR and reflectance-based VIs are not fully independent, which can result in a strong relation between MTVI2 and FY_{760} .

The reduced reabsorption effects of F_{687} under environmental stress resulted in a strong increase of the $F_{\rm ratio}$ and a moderate relationship with LUE under SC (Fig. 4). Since the $F_{\rm ratio}$ does not depend on a viable fAPAR estimation it is less affected by possible co-correlations and easier to obtain. Therefore, the signal shows potential in providing a simple way to derive information about chlorophyll content and plant stress responses (Middleton et al., 2017; Rossini et al., 2015; Wieneke et al., 2016).

4.3. De-trending of FY₇₆₀ and PRI

It is demonstrated that the observed seasonal trend in FY_{760} and PRI can be corrected by using the MTVI2 as a LAI proxy, where resulting rFY_{760} and rPRI show a relatively stable behavior over the season (Fig. 5). The weak relationship between intra-daily rFY_{760} with LUE

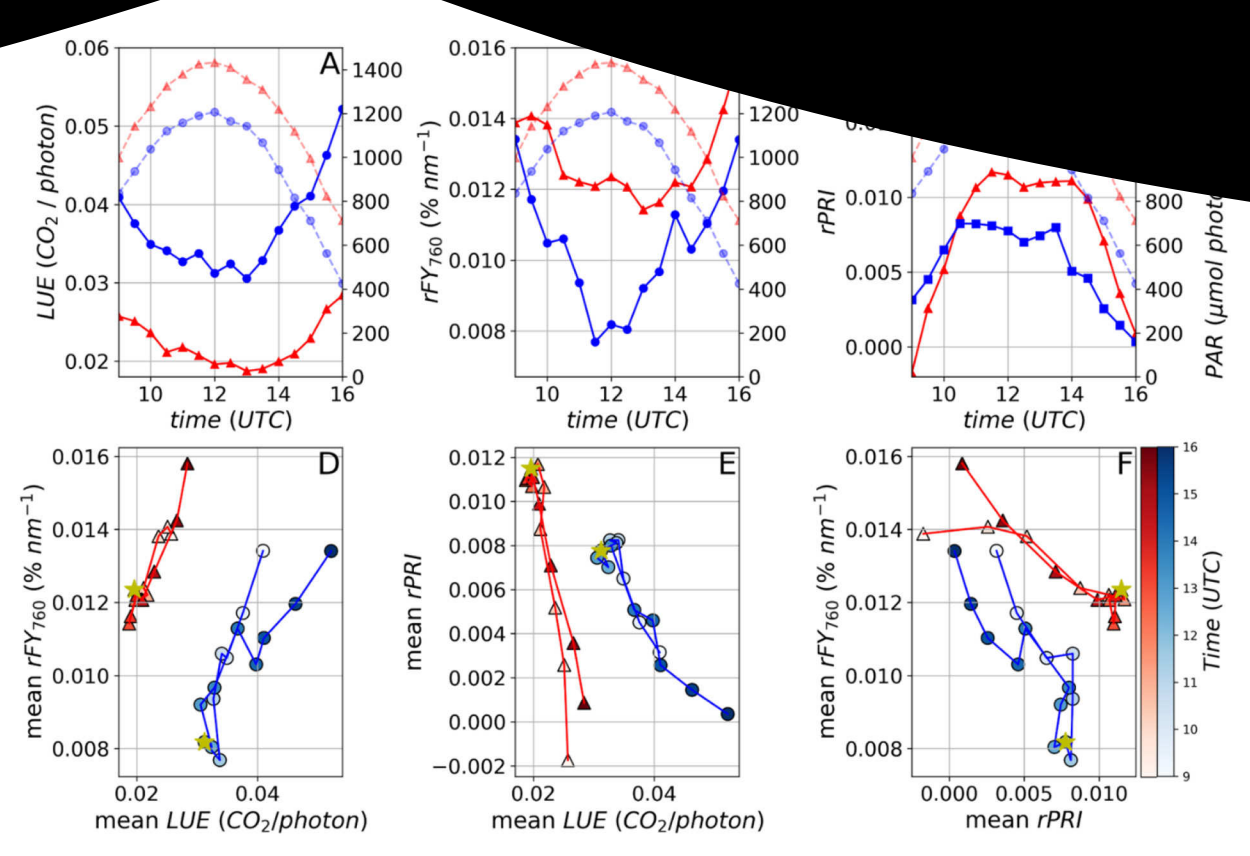


Fig. 7. Averaged diurnal cycles (A–C) and trajectories (D–F) of LUE, rFY₇₆₀ and rPRI under non-stresses conditions (NSC; 7 days average; blue dots) and under stressed conditions (SC; 17 days average; red dots). Days with diffuse light conditions were excluded. The color gradient of the dots represents the daytime, where lowest intensity represents 9 am and highest intensity 4 pm. The yellow star indicates solar noon. (For interpretation of the references to color in this figure legend, the reader is referred to the web version of this article.)

under SC and NSC can be explained by a stronger dispersion of rFY₇₆₀ caused by diurnal fluctuations (Fig. 6A). Once diurnal fluctuations are averaged out, the seasonal results show a stronger relationship between $\ensuremath{\mathrm{rFY}}_{760}$ and LUE under NSC and SC Fig. 6D. The reverse relationship of FY₇₆₀ to LUE (Fig. 4A & C), compared to the one of rFY₇₆₀ (Fig. 6D) indicates that seasonal structural changes of the canopy might outweigh physiological effects. In their review paper Porcar-Castell et al. (2014) claim that under constant NPO the relationship between PO and FY can be inverted. This might explain the relatively strong relationship between seasonal rFY and LUE under NSC but not as much the relationship under SC where rPRI shows a high activity (Fig. 6D & E). These results indicate that rFY760 might contain information about adaptations in the photosynthetic light reactions. The general increase of rPRI with decreasing LUE is related to a stronger xanthophyll activity under heat stress (Porcar-Castell et al., 2014, 2012), which also explains the stronger response of rPRI under SC (Fig. 6B).

4.4. Diurnal plant adaptation strategies

The results show that LUE decreases until around 1 h after solar noon, when normally temperature is highest (Fig. 7A). To prevent water loss by increased transpiration rates, the plant closes the stomata, which downregulates the $\rm CO_2$ assimilation rate of dark reactions. To prevent damage due to photorespiration the plant then downregulates the energy used for PQ by releasing energy in the form of heat (NPQ) (Porcar-Castell et al., 2014). After solar noon, the LUE starts to increase and usually reaches higher values in the late afternoon than in the morning (Fig. 7A). Under both NSC and SC, the LUE recovers nearly simultaneous with decreasing rPRI (Fig. 7A, C, E), which implies a decreasing release of light energy as heat (NPQ) accompanied by an increasing use of light energy for photosynthesis (PQ). Diurnal rFY₇₆₀

shows a faster and stronger increase after solar noon under NSC than under SC. Under NSC rFY760 seems to share a stronger link to the recovering LUE than under SC, where rFY760 increases only after rPRI decreases (Fig. 7A-C). The nearly identical relationships of stressed rFY₇₆₀, rPRI, and LUE before and after solar noon indicates a strong diurnal interdependency of these parameters (Fig. 7D-F). In contrast to the seasonal negative relationship between $\ensuremath{\mathrm{rFY}_{760}}$ and LUE (Fig. 6D), a positive one was found for the averaged diurnal data (Fig. 7D). Following the argumentation of Porcar-Castell et al. (2014) the positive relationship indicates a dynamic and dominant activity of NPQ. The higher values of rFY₇₆₀ under SC compared to NSC is in contradiction with many publications (e.g. Chaves, 1991; Flexas et al., 2002; Porcar-Castell et al., 2014) and is therefore most likely related to de-trending artefacts. The relationship found between rPRI and rFY760 agrees with findings by Alonso et al. (2017), where they show that leaf level FY₇₄₀ decreases with increasing NPQ. The closer relationship of rPRI to ${
m rFY}_{760}$ during SC (compared to NSC) indicates that rFY760 is stronger influenced by NPQ under environmental stress (Fig. 7F). However, further studies are needed to understand the diurnal and seasonal adaptation and competitive relationship between absorbed photosynthetic active radiation, photochemical quenching, fluorescence, and non-photochemical quenching using remote sensing techniques.

4.5. Remote sensing within the flux tower footprint

One of the main difficulties in comparing optical RS data with flux measurements is due to the differences in the spatial and temporal sampling scale. Liu et al. (2017) for example shows that with a bare fiber optic, a typical field of view (FOV) of 25° and a sensor height of 20 m only 1.9% of the flux footprint is covered. Since we perform our measurements at only 2 m height, the average flux tower footprint is

ancantly lower. Liu et al. (2017) suggest widening the FOV by using cosine receptors to 72° which increased the coverage of the flux footprint to 75.7%. However, it can be expected that a widening of the FOV would also result in a stronger influence of BRDF effects on the fluorescence retrieval and consequently increase measurement uncertainty. Studies which analyze the increasing uncertainty with increasing FOV have to be carried out to find a trade-off between spatial sampling scale and increased measurement uncertainty. Another difficulty in the comparison between optical and flux measurement is related to the low operational temporal resolution of EC systems. Even though the sampling time of EC systems are at 10 to 20 Hz, the data are aggregated to 30 min and miss therefore many fine-scale regulatory processes (e.g. NPO, fluorescence, PO) which might be detectable with optical sensors (Gamon, 2015). Even thought it might be possible to reduce the aggregation time from 30 min to 10 min a further decrease will result in higher uncertainties due to non-stationarity issues.

5. Conclusions

In this work a high-resolution spectrometer was used to measure red and far-red fluorescence and several reflectance indices over one growing season in 2015. Diurnal and seasonal dynamics were compared to ${\rm CO}_2$ assimilation rates derived from a close by EC tower.

A strong linear relationship between GPP and F_{760} was found for sugar beets plants. This strong relationship however is significantly reduced under drought stress conditions, and it is furthermore demonstrated that the relationship is mainly controlled by APAR. It is therefore recommend to use FY (APAR-independent) for the interpretation of photosynthetic adaptations within the light reactions.

Stress-induced changes in the leaf and canopy structure (e.g., leaf angle adjustments and movement (Arena et al., 2008; Kadioglu et al., 2012)) and chlorophyll content (Rossini et al., 2016; Van Wittenberghe et al., 2015) can reduce the re-absorption of red fluorescence. This results in a stronger F_{687} signal under SC and complicates therefore interpretation of diurnal and seasonal F_{687} . Since red- and far-red fluorescence have different contributions from the two photosystems (PSII and PSI), the ratio of the two signals might contain valuable information about photosynthetic adaptation strategies. The development of novel correction methods for a proper detection of both fluorescence peaks is therefore of high importance. However, the reduced reabsorption effects of F_{687} under drought conditions lead to a strong increase in the $F_{\rm ratio}$ (F_{687}/F_{760}), which then again can be used as an easy method to detect drought stress.

Even though APAR-independent FY_{760} showed to be a suitable predictor of seasonal LUE, it was found that this relationship is strongly influenced by seasonal changes in the canopy structure. Since APAR and VIs were measured by the same instrument it is not clear if the strong relationship between FY_{760} and MTVI2 is caused by an interrelation or if FY is in general affected by seasonal structural changes even though FY is relativized by APAR.

De-trended rFY₇₆₀ showed potential in estimating seasonal LUE under NSC and SC. Averaged diurnal trajectories furthermore demonstrated that rFY₇₆₀, rPRI and LUE share strong interdependencies in particular under SC. However, the correction method used in this work only accounts for seasonal changes in canopy structure and it is unclear how strong diurnal canopy effects influence the diurnal relationships. Therefore, it is proposed that more sophisticated methods (e.g. radiative transfer models) should be used to disentangle physiological from structural signals.

All in all no unique relationship between fluorescence and photochemical efficiency could be established. This could be related to structural effects but also to dynamic non-radiative dissipation of excitation energy which is dynamic and under physiological control. Stress factors that may occur under natural environmental conditions can induce different responses of fluorescence emission and NPQ. Natural stress factors generally induce a reduction of photosynthetic

ferent stress factorstraightforward due to the co-

Furthermore, it has to be noted that the results are sore; measurements over sugar beet and over a single season. To fully assess the potential of F as an indicator for plant adaptation strategies additional measurements over different targets in different scales and several seasons are needed.

Acknowledgements

We gratefully thank the Transregional Collaborative Research Centre 32 "Patterns in Soil-Vegetation-Atmosphere-Systems" (TR32/2 2011 3009725), funded by the German Research Foundation (DFG) for facilitating our research. Cendrero-Mateo M.P. is currently funded by AVANFLEX project (Advanced Products for the FLEX mission), no ESP2016-79503-C2-1-P, Ministry of Economy and Competitiveness, Spain.

We especially thank Rainer Haseneder-Lind for the assembling of the SIF-Sys measurement system, Alexander Graf for the provision of the gap filled EC data, and Susanne Crewell, Karl Schneider, Matthias Langensiepen and Ana Bastos for their support and valuable contribution and discussions.

Appendix A. Supplementary Figures

Supplementary data to this article can be found online at https://doi.org/10.1016/j.rse.2018.10.019.

References

- Ač, A., Malenovský, Z., Olejníčková, J., Gallé, A., Rascher, U., Mohammed, G., 2015. Meta-analysis assessing potential of steady-state chlorophyll fluorescence for remote sensing detection of plant water, temperature and nitrogen stress. Remote Sens. Environ. 168, 420–436. https://doi.org/10.1016/j.rse.2015.07.022.
- Alonso, L., Gomez-Chova, L., Vila-Frances, J., Amoros-Lopez, J., Guanter, L., Calpe, J., Moreno, J., 2008. Improved Fraunhofer line discrimination method for vegetation fluorescence quantification. IEEE Geosci. Remote Sens. Lett. 5, 620–624. https://doi. org/10.1109/JGRS.2008.2001180.
- Alonso, L., Van Wittenberghe, S., Amorós-López, J., Vila-Francés, J., Gómez-Chova, L., Moreno, J., 2017. Diurnal cycle relationships between passive fluorescence, PRI and NPQ of vegetation in a controlled stress experiment. Remote Sens. 9, 770. https:// doi.org/10.3390/rs9080770.
- Arena, C., Vitale, L., Santo, A.V.D., 2008. Paraheliotropism in *Robinia pseudoacacia* plants: an efficient means to cope with photoinhibition. In: Allen, J.F., Gantt, E., Golbeck, J.H., Osmond, B. (Eds.), Photosynthesis. Energy from the Sun. Springer, Netherlands, pp. 1403–1406. https://doi.org/10.1007/978-1-4020-6709-9_302.
- Baker, N.R., 2008. Chlorophyll fluorescence: a probe of photosynthesis in vivo. Annu. Rev. Plant Biol. 59, 89–113. https://doi.org/10.1146/annurev.arplant.59.032607. 092759
- Baldocchi, D.D., 2003. Assessing the eddy covariance technique for evaluating carbon dioxide exchange rates of ecosystems: past, present and future. Glob. Chang. Biol. 9, 479–492. https://doi.org/10.1046/j.1365-2486.2003.00629.x.
- Barton, C.V.M., North, P.R.J., 2001. Remote sensing of canopy light use efficiency using the photochemical reflectance index: model and sensitivity analysis. Remote Sens. Environ. 78, 264–273. https://doi.org/10.1016/S0034-4257(01)00224-3.
- Burkart, A., Schickling, A., Mateo, M.P.C., Wrobel, T.J., Rossini, M., Cogliati, S., Julitta, T., Rascher, U., 2015. A method for uncertainty assessment of passive sun-induced chlorophyll fluorescence retrieval using an infrared reference light. IEEE Sensors J. 15, 4603–4611. https://doi.org/10.1109/JSEN.2015.2422894.
- Chaves, M.M., 1991. Effects of water deficits on carbon assimilation. J. Exp. Bot. 42, 1–16. https://doi.org/10.1093/jxb/42.1.1.
- Cheng, Y.-B., Middleton, E.M., Zhang, Q., Huemmrich, K.F., Campbell, P.K.E., Corp, L.A., Cook, B.D., Kustas, W.P., Daughtry, C.S., 2013. Integrating solar induced fluorescence and the photochemical reflectance index for estimating gross primary production in a cornfield. Remote Sens. 5, 6857–6879. https://doi.org/10.3390/rs5126857.
- Ciais, P., Sabine, C., Bala, G., Bopp, L., Brovkin, V., Canadell, J., Chhabra, A., DeFries, R., Galloway, J., Heimann, M., et al., 2014. Carbon and other biogeochemical cycles. In: Climate Change 2013: the Physical Science Basis. Contribution of Working Group I to the Fifth Assessment Report of the Intergovernmental Panel on Climate Change. Cambridge University Press, pp. 465–570.
- Cogliati, S., Rossini, M., Julitta, T., Meroni, M., Schickling, A., Burkart, A., Pinto, F., Rascher, U., Colombo, R., 2015. Continuous and long-term measurements of

- reflectance and sun-induced chlorophyll fluorescence by using novel automated field spectroscopy systems. Remote Sens. Environ. 164, 270–281. https://doi.org/10.1016/j.rse.2015.03.027.
- Damm, A., Guanter, L., Laurent, V.C.E., Schaepman, M.E., Schickling, A., Rascher, U., 2014. FLD-based retrieval of sun-induced chlorophyll fluorescence from medium spectral resolution airborne spectroscopy data. Remote Sens. Environ. 147, 256–266. https://doi.org/10.1016/j.rse.2014.03.009.
- Damm, A., Guanter, L., Verhoef, W., Schläpfer, D., Garbari, S., Schaepman, M.E., 2015. Impact of varying irradiance on vegetation indices and chlorophyll fluorescence derived from spectroscopy data. Remote Sens. Environ. 156, 202–215. https://doi. org/10.1016/j.rse.2014.09.031.
- Drolet, G.G., Huemmrich, K.F., Hall, F.G., Middleton, E.M., Black, T.A., Barr, A.G., Margolis, H.A., 2005. A MODIS-derived photochemical reflectance index to detect inter-annual variations in the photosynthetic light-use efficiency of a boreal deciduous forest. Remote Sens. Environ. 98, 212–224. https://doi.org/10.1016/j.rse.2005.07.006.
- Drolet, G.G., Middleton, E.M., Huemmrich, K.F., Hall, F.G., Amiro, B.D., Barr, A.G., Black, T.A., McCaughey, J.H., Margolis, H.A., 2008. Regional mapping of gross light-use efficiency using MODIS spectral indices. Remote Sens. Environ. 112, 3064–3078. https://doi.org/10.1016/j.rse.2008.03.002.
- Du, S., Liu, L., Liu, X., Hu, J., 2017. Response of canopy solar-induced chlorophyll fluorescence to the absorbed photosynthetically active radiation absorbed by chlorophyll. Remote Sens. 9, 911. https://doi.org/10.3390/rs9090911.
- Farquhar, G.D., von Caemmerer, S., Berry, J.A., 2001. Models of photosynthesis. Plant Physiol. 125, 42–45. https://doi.org/10.1104/pp.125.1.42.
- Flexas, J., Escalona, J.M., Evain, S., Gulías, J., Moya, I., Osmond, C.B., Medrano, H., 2002. Steady-state chlorophyll fluorescence (fs) measurements as a tool to follow variations of net CO2 assimilation and stomatal conductance during water-stress in C3 plants. Physiol. Plant. 114, 231–240. https://doi.org/10.1034/j.1399-3054.2002. 1140209.x.
- Fournier, A., Daumard, F., Champagne, S., Ounis, A., Goulas, Y., Moya, I., 2012. Effect of canopy structure on sun-induced chlorophyll fluorescence. ISPRS J. Photogramm. Remote Sens. 68, 112–120. https://doi.org/10.1016/j.isprsjprs.2012.01.003.
- Frankenberg, C., Fisher, J.B., Worden, J., Badgley, G., Saatchi, S.S., Lee, J.-E., Toon, G.C., Butz, A., Jung, M., Kuze, A., Yokota, T., 2011. New global observations of the terrestrial carbon cycle from GOSAT: patterns of plant fluorescence with gross primary productivity. Geophys. Res. Lett. 38, L17706. https://doi.org/10.1029/ 2011GI.048738.
- Frankenberg, C., O'Dell, C., Berry, J., Guanter, L., Joiner, J., Koehler, P., Pollock, R., Taylor, T.E., 2014. Prospects for chlorophyll fluorescence remote sensing from the orbiting carbon observatory-2. Remote Sens. Environ. 147, 1–12. https://doi.org/10. 1016/i.rse.2014.02.007.
- $\label{eq:Gamon, J.A., 2015. Reviews and syntheses: optical sampling of the flux tower footprint. \\ Biogeosciences 12, 4509–4523. \\ https://doi.org/10.5194/bg-12-4509-2015.$
- Gamon, J.A., Peñuelas, J., Field, C.B., 1992. A narrow-waveband spectral index that tracks diurnal changes in photosynthetic efficiency. Remote Sens. Environ. 41, 35–44. https://doi.org/10.1016/0034-4257(92)90059-S.
- Gamon, J.A., Field, C.B., Fredeen, A.L., Thayer, S., 2001. Assessing photosynthetic downregulation in sunflower stands with an optically-based model. Photosynth. Res. 67, 113–125. https://doi.org/10.1023/A:1010677605091.
- Gitelson, A.A., Gamon, J.A., Solovchenko, A., 2017. Multiple drivers of seasonal change in PRI: implications for photosynthesis 2. Stand level. Remote Sens. Environ. 190, 198–206. https://doi.org/10.1016/j.rse.2016.12.015.
- Goulas, Y., Fournier, A., Daumard, F., Champagne, S., Ounis, A., Marloie, O., Moya, I., 2017. Gross primary production of a wheat canopy relates stronger to far red than to red solar-induced chlorophyll fluorescence. Remote Sens. 9, 97. https://doi.org/10. 3390/rs9010097.
- Graf, A., Werner, J., Langensiepen, M., van de Boer, A., Schmidt, M., Kupisch, M., Vereecken, H., 2013. Validation of a minimum microclimate disturbance chamber for net ecosystem flux measurements. Agric. For. Meteorol. 174–175, 1–14. https://doi. org/10.1016/j.agrformet.2013.02.001.
- Guanter, L., Frankenberg, C., Dudhia, A., Lewis, P.E., Gómez-Dans, J., Kuze, A., Suto, H., Grainger, R.G., 2012. Retrieval and global assessment of terrestrial chlorophyll fluorescence from GOSAT space measurements. Remote Sens. Environ. 121, 236–251. https://doi.org/10.1016/j.rse.2012.02.006.
- Guanter, L., Zhang, Y., Jung, M., Joiner, J., Voigt, M., Berry, J.A., Frankenberg, C., Huete, A.R., Zarco-Tejada, P., Lee, J.-E., Moran, M.S., Ponce-Campos, G., Beer, C., Camps-Valls, G., Buchmann, N., Gianelle, D., Klumpp, K., Cescatti, A., Baker, J.M., Griffis, T.J., 2014. Global and time-resolved monitoring of crop photosynthesis with chlorophyll fluorescence. Proc. Natl. Acad. Sci. 111, E1327–E1333. https://doi.org/10.1073/pnas.1320008111.
- Guofang, M., Kaiyu, G., Xi, Y., BC, J., BJ, A., DE, H., Jin, W., MC, E., Katherine, M., Yaping, C., Bin, P., Hyungsuk, K., MM, D., 2018. Sun-induced chlorophyll fluorescence, photosynthesis, and light use efficiency of a soybean field from seasonally continuous measurements. J. Geophys. Res. Biogeosci. 123, 610–623. https://doi.org/10.1002/2017JG004180.
- Haboudane, D., Miller, J.R., Pattey, E., Zarco-Tejada, P.J., Strachan, I.B., 2004.
 Hyperspectral vegetation indices and novel algorithms for predicting green LAI of crop canopies: modeling and validation in the context of precision agriculture.
 Remote Sens. Environ. 90, 337–352. https://doi.org/10.1016/j.rse.2003.12.013.
- Joiner, J., Yoshida, Y., Vasilkov, A.P., Yoshida, Y., Corp, L.A., Middleton, E.M., 2011. First observations of global and seasonal terrestrial chlorophyll fluorescence from space. Biogeosciences 8, 637–651. https://doi.org/10.5194/bg-8-637-2011.
- Joiner, J., Yoshida, Y., Vasilkov, A.P., Middleton, E.M., Campbell, P.K.E., Yoshida, Y., Kuze, A., Corp, L.A., 2012. Filling-in of near-infrared solar lines by terrestrial fluorescence and other geophysical effects: simulations and space-based observations from

- Joiner, J., Guan.
 Huemmrich, K.F., Yos...
 chlorophyll fluorescence from floc.
 measurements: methodology, simulations, and approximately.
 Tech. 6, 2803–2823. https://doi.org/10.5194/amt-6-2803-
- Julitta, T., Corp, L.A., Rossini, M., Burkart, A., Cogliati, S., Davies, N., Hom, M., Arthur, A., Middleton, E.M., Rascher, U., Schickling, A., Colombo, R., 2016.
 Comparison of sun-induced chlorophyll fluorescence estimates obtained from four portable field spectroradiometers. Remote Sens. 8, 122. https://doi.org/10.3390/rs8020122
- Kadioglu, A., Terzi, R., Saruhan, N., Saglam, A., 2012. Current advances in the investigation of leaf rolling caused by biotic and abiotic stress factors. Plant Sci. 182, 42–48. https://doi.org/10.1016/j.plantsci.2011.01.013. Abiotic stress tolerances.
- Köhler, P., Guanter, L., Joiner, J., 2015. A linear method for the retrieval of sun-induced chlorophyll fluorescence from GOME-2 and SCIAMACHY data. Atmos. Meas. Tech. 8, 2589–2608. https://doi.org/10.5194/amt-8-2589-2015.
- Kolber, Z., Klimov, D., Ananyev, G., Rascher, U., Berry, J., Osmond, B., 2005. Measuring photosynthetic parameters at a distance: laser induced fluorescence transient (LIFT) method for remote measurements of photosynthesis in terrestrial vegetation. Photosynth. Res. 84, 121–129. https://doi.org/10.1007/s11120-005-5092-1.
- Li, Z., Moreau, L., 1996. A new approach for remote sensing of canopy-absorbed photosynthetically active radiation. I: Total surface absorption. Remote Sens. Environ. 55, 175–191. https://doi.org/10.1016/S0034-4257(95)00097-6.
- Li, X., Xiao, J., He, B., 2018. Chlorophyll fluorescence observed by OCO-2 is strongly related to gross primary productivity estimated from flux towers in temperate forests. Remote Sens. Environ. 204, 659–671. https://doi.org/10.1016/j.rse.2017.09.034.
- Lichtenthaler, H.K., Rinderle, U., 1988. The role of chlorophyll fluorescence in the detection of stress conditions in plants. CRC Crit. Rev. Anal. Chem. 19, S29–S85. https://doi.org/10.1080/15476510.1988.10401466.
- Lichtenthaler, H.K., Hak, R., Rinderle, U., 1990. The chlorophyll fluorescence ratio F690/F730 in leaves of different chlorophyll content. Photosynth. Res. 25, 295–298. https://doi.org/10.1007/BF00033170.
- Liu, X., Liu, L., Hu, J., Du, S., 2017. Modeling the footprint and equivalent radiance transfer path length for tower-based hemispherical observations of chlorophyll fluorescence. Sensors 17, 1131. https://doi.org/10.3390/s17051131.
- Mauder, M., Foken, T., 2015. Documentation and instruction manual of the eddy-covariance software package TK3 (update).
- Mauder, M., Cuntz, M., Drüe, C., Graf, A., Rebmann, C., Schmid, H.P., Schmidt, M., Steinbrecher, R., 2013. A strategy for quality and uncertainty assessment of long-term eddy-covariance measurements. Agric. For. Meteorol. 169, 122–135. https://doi.org/ 10.1016/j.agrformet.2012.09.006.
- Maxwell, K., Johnson, G.N., 2000. Chlorophyll fluorescence—a practical guide. J. Exp. Bot. 51, 659–668.
- Meroni, M., Rossini, M., Guanter, L., Alonso, L., Rascher, U., Colombo, R., Moreno, J., 2009. Remote sensing of solar-induced chlorophyll fluorescence: review of methods and applications. Remote Sens. Environ. 113, 2037–2051. https://doi.org/10.1016/j. rse.2009.05.003.
- Middleton, E.M., Rascher, U., Corp, L.A., Huemmrich, K.F., Cook, B.D., Noormets, A., Schickling, A., Pinto, F., Alonso, L., Damm, A., Guanter, L., Colombo, R., Campbell, P.K.E., Landis, D.R., Zhang, Q., Rossini, M., Schuettemeyer, D., Bianchi, R., 2017. The 2013 FLEX—US airborne campaign at the Parker tract loblolly pine plantation in North Carolina, USA. Remote Sens. 9, 612. https://doi.org/10.3390/rs9060612.
- Orth, R., Zscheischler, J., Seneviratne, S.I., 2016. Record dry summer in 2015 challenges precipitation projections in Central Europe. Sci. Rep. 6. https://doi.org/10.1038/ srep28334.
- Papageorgiou, G.C., Govindjee, 2004. Chlorophyll a fluorescence a signature of photosynthesis. | G.C. Papageorgiou | Springer. Springer Netherlands, Dordrecht.
- Peñuelas, J., Garbulsky, M.F., Filella, I., 2011. Photochemical reflectance index (PRI) and remote sensing of plant CO₂ uptake. New Phytol. 191, 596–599. https://doi.org/10. 1111/j.1469-8137.2011.03791.x.
- Plascyk, J.A., Gabriel, F.C., 1975. The fraunhofer line discriminator MKII-an airborne instrument for precise and standardized ecological luminescence measurement. IEEE Trans. Instrum. Meas. 24, 306–313. https://doi.org/10.1109/TIM.1975.4314448.
- Porcar-Castell, A., Garcia-Plazaola, J.I., Nichol, C.J., Kolari, P., Olascoaga, B., Kuusinen, N., Fernández-Marín, B., Pulkkinen, M., Juurola, E., Nikinmaa, E., 2012. Physiology of the seasonal relationship between the photochemical reflectance index and photosynthetic light use efficiency. Oecologia 170, 313–323. https://doi.org/10.1007/s00442-012-2317-9.
- Porcar-Castell, A., Tyystjärvi, E., Atherton, J., van der Tol, C., Flexas, J., Pfündel, E.E., Moreno, J., Frankenberg, C., Berry, J.A., 2014. Linking chlorophyll a fluorescence to photosynthesis for remote sensing applications: mechanisms and challenges. J. Exp. Bot. https://doi.org/10.1093/jxb/eru191. (eru191).
- Rascher, U., Alonso, L., Burkart, A., Cilia, C., Cogliati, S., Colombo, R., Damm, A., Drusch, M., Guanter, L., Hanus, J., Hyvärinen, T., Julitta, T., Jussila, J., Kataja, K., Kokkalis, P., Kraft, S., Kraska, T., Matveeva, M., Moreno, J., Muller, O., Panigada, C., Pikl, M., Pinto, F., Prey, L., Pude, R., Rossini, M., Schickling, A., Schurr, U., Schüttemeyer, D., Verrelst, J., Zemek, F., 2015. Sun-induced fluorescence a new probe of photosynthesis: first maps from the imaging spectrometer HyPlant. Glob. Chang. Biol. https://doi.org/10.1111/gcb.13017.
- Reichstein, M., Falge, E., Baldocchi, D., Papale, D., Aubinet, M., Berbigier, P., Bernhofer, C., Buchmann, N., Gilmanov, T., Granier, A., Grünwald, T., Havránková, K., Ilvesniemi, H., Janous, D., Knohl, A., Laurila, T., Lohila, A., Loustau, D., Matteucci, G., Meyers, T., Miglietta, F., Ourcival, J.-M., Pumpanen, J., Rambal, S., Rotenberg, E., Sanz, M., Tenhunen, J., Seufert, G., Vaccari, F., Vesala, T., Yakir, D., Valentini, R.,

- 2005. On the separation of net ecosystem exchange into assimilation and ecosystem respiration: review and improved algorithm. Glob. Chang. Biol. 11, 1424–1439 https://doi.org/10.1111/j.1365-2486.2005.001002.x.
- Rossini, M., Meroni, M., Migliavacca, M., Manca, G., Cogliati, S., Busetto, L., Picchi, V., Cescatti, A., Seufert, G., Colombo, R., 2010. High resolution field spectroscopy measurements for estimating gross ecosystem production in a rice field. Agric. For. Meteorol. 150, 1283–1296. https://doi.org/10.1016/j.agrformet.2010.05.011.
- Rossini, M., Nedbal, L., Guanter, L., Ač, A., Alonso, L., Burkart, A., Cogliati, S., Colombo, R., Damm, A., Drusch, M., Hanus, J., Janoutova, R., Julitta, T., Kokkalis, P., Moreno, J., Novotny, J., Panigada, C., Pinto, F., Schickling, A., Schüttemeyer, D., Zemek, F., Rascher, U., 2015. Red and far red sun-induced chlorophyll fluorescence as a measure of plant photosynthesis. Geophys. Res. Lett. 42https://doi.org/10.1002/2014GL062943. (2014GL062943).
- Rossini, M., Meroni, M., Celesti, M., Cogliati, S., Julitta, T., Panigada, C., Rascher, U., van der Tol, C., Colombo, R., 2016. Analysis of red and far-red sun-induced chlorophyll fluorescence and their ratio in different canopies based on observed and modeled data. Remote Sens. 8, 412. https://doi.org/10.3390/rs8050412.
- Schreiber, U., 2004. Pulse-amplitude-modulation (PAM) fluorometry and saturation pulse method: an overview. In: Papageorgiou, G.C., Govindjee (Eds.), Chlorophyll a Fluorescence, Advances in Photosynthesis and Respiration. Springer Netherlands, pp. 279–319. https://doi.org/10.1007/978-1-4020-3218-9 11.
- Sims, D.A., Gamon, J.A., 2002. Relationships between leaf pigment content and spectral reflectance across a wide range of species, leaf structures and developmental stages. Remote Sens. Environ. 81, 337–354. https://doi.org/10.1016/S0034-4257(02) 00010-X.
- Sun, Y., Frankenberg, C., Jung, M., Joiner, J., Guanter, L., Köhler, P., Magney, T., 2018. Overview of solar-induced chlorophyll fluorescence (SIF) from the orbiting carbon observatory-2: retrieval, cross-mission comparison, and global monitoring for GPP. Remote Sens. Environ. https://doi.org/10.1016/j.rse.2018.02.016.
- Van Wittenberghe, S., Alonso, L., Verrelst, J., Hermans, I., Delegido, J., Veroustraete, F., Valcke, R., Moreno, J., Samson, R., 2013. Upward and downward solar-induced chlorophyll fluorescence yield indices of four tree species as indicators of traffic pollution in Valencia. Environ. Pollut. 173, 29–37. https://doi.org/10.1016/j.envpol. 2012.10.003.
- Van Wittenberghe, S., Alonso, L., Verrelst, J., Moreno, J., Samson, R., 2015. Bidirectional sun-induced chlorophyll fluorescence emission is influenced by leaf structure and light scattering properties — a bottom-up approach. Remote Sens. Environ. 158,

- at the canop
- Wieneke, S., Ahrends, H., Damm, A., T.,
 Airborne based spectroscopy of red and far-red simplications for improved estimates of gross primary productions. https://doi.org/10.1016/j.rse.2016.07.025.
- Wu, C., Niu, Z., Tang, Q., Huang, W., 2010. Revised photochemical reflectance index (PRI) for predicting light use efficiency of wheat in a growth cycle: validation and comparison. Int. J. Remote Sens. 31, 2911–2924. https://doi.org/10.1080/ 01431160903121118.
- Wu, C., Huang, W., Yang, Q., Xie, Q., 2015. Improved estimation of light use efficiency by removal of canopy structural effect from the photochemical reflectance index (PRI). Agric. Ecosyst. Environ. 199, 333–338. https://doi.org/10.1016/j.agee.2014.10.017.
- Zacharias, S., Bogena, H., Samaniego, L., Mauder, M., Fuß, R., Pütz, T., Frenzel, M., Schwank, M., Baessler, C., Butterbach-Bahl, K., Bens, O., Borg, E., Brauer, A., Dietrich, P., Hajnsek, I., Helle, G., Kiese, R., Kunstmann, H., Klotz, S., Munch, J.C., Papen, H., Priesack, E., Schmid, H.P., Steinbrecher, R., Rosenbaum, U., Teutsch, G., Vereecken, H., 2011. A Network of Terrestrial Environmental Observatories in Germany. Vadose Zone J. 10, 955–973 https://doi.org/10.2136/vzj2010.0139.
- Zarco-Tejada, P.J., Berni, J.A.J., Suárez, L., Sepulcre-Cantó, G., Morales, F., Miller, J.R., 2009. Imaging chlorophyll fluorescence with an airborne narrow-band multispectral camera for vegetation stress detection. Remote Sens. Environ. 113, 1262–1275. https://doi.org/10.1016/j.rse.2009.02.016.
- Zhang, Yao, Xiao, X., Jin, C., Dong, J., Zhou, S., Wagle, P., Joiner, J., Guanter, L., Zhang, Yongguang, Zhang, G., Qin, Y., Wang, J., Moore, B., 2016. Consistency between sun-induced chlorophyll fluorescence and gross primary production of vegetation in North America. Remote Sens. Environ. 183, 154–169. https://doi.org/10.1016/j.rse. 2016.05.015.
- Zhang, Yao, Xiao, X., Zhang, Yongguang, Wolf, S., Zhou, S., Joiner, J., Guanter, L., Verma, M., Sun, Y., Yang, X., Paul-Limoges, E., Gough, C.M., Wohlfahrt, G., Gioli, B., van der Tol, C., Yann, N., Lund, M., de Grandcourt, A., 2018. On the relationship between sub-daily instantaneous and daily total gross primary production: implications for interpreting satellite-based SIF retrievals. Remote Sens. Environ. 205, 276–289. https://doi.org/10.1016/j.rse.2017.12.009.